Environmental Science & Technology

pubs.acs.org/est

Article

Synergistic Catalytic Elimination of NO_x and Chlorinated Organics: Cooperation of Acid Sites

Chi Zhang, Jianping Zhang, Yongjie Shen, Jiebing He, Wenqiang Qu, Jiang Deng, Lupeng Han, Aling Chen,* and Dengsong Zhang*

Cite This: *Environ. Sci. Technol.* 2022, 56, 3719−3728

Read Online

ACCESS | Metrics & More | Article Recommendations | Supporting Information

ABSTRACT: The synergistic catalytic removal of NO_x and chlorinated volatile organic compounds under low temperatures is still a big challenge. Generally, degradation of chlorinated organics demands sufficient redox ability, which leads to low N_2 selectivity in the selective catalytic reduction of NO_x by NH_3 (NH_3-SCR). Herein, mediating acid sites *via* introducing the $CePO_4$ component into MnO_2/TiO_2 NH_3-SCR catalysts was found to be an effective approach for promoting chlorobenzene degradation. The observation of *in situ* diffuse reflectance infrared Fourier transform (*in situ* DRIFT) and Raman spectra reflected that the Lewis acid sites over $CePO_4$ promoted the nucleophilic substitution process of chlorobenzene over MnO_2 by weakening the bond between Cl and benzene ring. Meanwhile, MnO_2 provided adequate Brønsted acid sites and redox sites. Under the cooperation of Lewis and Brønsted acid sites, relying on the rational redox ability, chlorobenzene degradation was promoted with synergistically improved NH_3-SCR activity and selectivity. This work offers a distinct pathway for promoting the combination of chlorobenzene catalytic oxidation and NH_3-SCR, and is expected to provide a novel strategy for synergistic catalytic elimination of NO_x and chlorinated volatile organic compounds.

KEYWORDS: *air pollution control, synergistic catalytic elimination, NO_x reduction, chlorinated organics*

1. INTRODUCTION

Both nitrogen oxides (NO_x) and polychlorodibenzo-*p*-dioxins/polychloro-dibenzofurans (PCDD/Fs) are emitted from especially the municipal and medical solid waste incineration and the steel industry,[1] which are toxic biologically and able to form photochemical smog.[2,3] As the emission standards become more stringent, the multipollutant control of NO_x and PCDD/Fs simulated by chlorobenzene (CB) attracts extensive attention. The catalysts for selective catalytic reduction of NO_x with NH_3 (NH_3-SCR) have been widely studied, and the typical V_2O_5−WO_3/TiO_2 catalysts have been exploited commercially.[4] NH_3-SCR catalysts always exhibit coupled acidity and redox properties, of which the Brønsted acid site is also the key factor for nucleophilic substitution that is the triggered step of degradation of CB, and the redox ability is the requisite for the further oxidation of the intermediates.[5,6] Therefore, the NH_3-SCR catalysts are expected to synergistically eliminate CB.

However, over the current well-known NH_3-SCR catalysts, the temperature window of NH_3-SCR is difficult to match the CB conversion temperature.[7,8] Generally, the redox ability of the NH_3-SCR catalyst is insufficient, which will result in higher CB conversion temperature, low CO_2 selectivity, and more incompletely oxidized products including regenerated PCDD/Fs.[9] Numerous efforts have been focused on VO_x-based catalysts recently, especially VO_x/TiO_2-based catalysts are considered as promising candidates for simultaneously eliminating NO_x and chlorinated organics.[10−12] The V_2O_5−MoO_3/TiO_2 catalyst investigated by Huang et al.[13] exhibited activity with 100% NO conversion within 200−400 °C and more than 90% CB conversion above 300 °C. However, the N_2 selectivity dramatically decreased above 300 °C. For V_2O_5−WO_3/TiO_2 catalysts, the CB and NO_x conversion reached 90% above 325 °C but with approximately 50% CO_2 selectivity, which might be due to the insufficient redox ability.[1] The dopant of Al_2O_3 into CeO_2 decreased the 80% CB conversion temperature from 335 to 274 °C by enhancing the redox ability.[14] The study about MnO_x−CeO_2 catalysts found that the CB conversion temperature could be reduced (completely eliminated at 300 °C) by enhanced redox ability but with poor N_2 selectivity.[5] Thus, the enhanced redox ability of the catalyst

Received: November 24, 2021
Revised: January 26, 2022
Accepted: February 16, 2022
Published: February 28, 2022

https://doi.org/10.1021/acs.est.1c08009
Environ. Sci. Technol. 2022, 56, 3719−3728

is beneficial for the activity and selectivity of CB conversion. Nevertheless, it also leads to more N_2O and NO production in NH_3-SCR.[5,7,15] Besides the redox ability, the positive effects of the Brønsted acid sites and H_2O for CB degradation have been realized in previous investigations.[13,16,17] Dai et al.[18] synthesized phosphoric acid-modified CeO_2 nanorods for CB catalytic oxidation (CBCO) with abundant Brønsted acid sites, which promoted the hydrolytic destruction of CB effectively at 250 °C, and also the addition of H_2O alleviated the Cl poisoning in the presence of Brønsted acid sites. However, developing catalysts with optimum redox ability and proper acid sites that could simultaneously lower CB degradation temperature and retain NH_3-SCR selectivity is still a huge challenge.

To balance N_2 selectivity with the CB conversion and CO_2 selectivity, lowering the CB conversion temperature without enhancing the redox ability could be an effective approach. With rational redox ability, taking advantage of the acid sites to decrease the CB conversion temperature to meet the NH_3-SCR temperature window could prevent the decrease of N_2 selectivity and sustain high CO_2 selectivity. In this work, dual active sites of MnO_2 and $CePO_4$ were constructed on MnO_2−$CePO_4/TiO_2$ catalysts to gain insight into the roles of Brønsted acid sites, Lewis acid sites, and redox sites in the synergistically catalytic elimination of NO_x and CB. The multipollutant conversion efficiency, synergistic effects, and mechanisms of reaction and poisoning were evaluated. Under the circumstances that the Brønsted acid sites have been proved to trigger the CB degradation by nucleophilic substitution,[18,19] this study found that Lewis acid sites were able to cooperate with Brønsted acid sites, which would facilitate the nucleophilic substitution process of CB. As a result, under the cooperation of the Lewis and Brønsted acid sites, the CBCO was promoted under lower temperatures without decaying the N_2 selectivity. This work might offer new guidance for designing efficient catalysts for the synergistic elimination of chlorinated organics and NO_x.

2. EXPERIMENTAL SECTION

2.1. Catalyst Preparation. In a typical preparation process, the MnO_2−$CePO_4/TiO_2$ catalyst with a Mn/Ce molar ratio of 4:6 was prepared through two steps. First, the $CePO_4$ over TiO_2 was prepared through the sol−gel method. $Ce(NO)_3{\cdot}6H_2O$ (0.30 g) was dissolved in deionized water, and then 1.80 g of TiO_2 was dispersed into the solution. After stirring for 20 min, a stoichiometric 0.079 g of H_3PO_4 was dribbled into the solution under continuous stirring, then $NH_3{\cdot}H_2O$ was added into the mixture till a solution of pH 9−10 was obtained. The mixture was kept under stirring for 1 h before aging in air at 30 °C for 48 h. The obtained precipitate after aging was washed and filtered by deionized water, followed by drying at 80 °C for 10 h. Second, manganese oxide was introduced onto the dried solid by the impregnation method and 0.11 g of $Mn(NO_3)_2{\cdot}4H_2O$ was impregnated by a rotary evaporator. Subsequently, the entirety was transferred to an oven at 80 °C for 4 h followed by calcining at 450 °C for 4 h. The MnO_2−$CePO_4/TiO_2$ catalysts with various molar ratios were prepared through the same method. For comparison, MnO_2/TiO_2 and $CePO_4/TiO_2$ catalysts with 10 wt % loading were prepared by the same method. MnO_2/TiO_2 and $CePO_4/TiO_2$ catalysts with the same MnO_2 (2 wt %) and $CePO_4$ (8 wt %) loading as that in MnO_2−$CePO_4/TiO_2$ were denoted as $CePO_4/TiO_2$ C and MnO_2/TiO_2 C, respectively. And the MnO_2−$CePO_4/TiO_2$ catalysts acquired after exposure to simultaneous NH_3-SCR and CBCO circumstances for 90 min were denoted as MnO_2−$CePO_4/TiO_2$-Cl. The MnO_2−$CePO_4$ catalyst with a Mn/Ce molar ratio of 4:6 was prepared with the same method as the synthesis of MnO_2−$CePO_4/TiO_2$ without TiO_2. The preparation details of all catalysts can be found in the Supporting Information (SI).

2.2. Performance Measurements. The gas mixture was composed of 500 ppm of NO, 500 ppm of NH_3, 5 vol % O_2, 100 ppm of CB, and N_2 balance. The total flow rate was 250 mL min^{-1}, and the gas hourly space velocity (GHSV) was about 50 000 mL g^{-1} h^{-1}. The NO and CB conversion rates were calculated by the following equation

$$\mathrm{NO}_x\ \text{conversion}(\%) = \frac{[\mathrm{NO}_x]_{\mathrm{in}} - [\mathrm{NO}_x]_{\mathrm{out}}}{[\mathrm{NO}_x]_{\mathrm{in}}} \times 100\%$$

$$\mathrm{N}_2\ \text{selectivity}(\%) = \left(1 - \frac{2[\mathrm{N}_2\mathrm{O}]}{[\mathrm{NH}_3]_{\mathrm{in}} + [\mathrm{NO}_x]_{\mathrm{in}} - [\mathrm{NH}_3]_{\mathrm{out}} - [\mathrm{NO}_x]_{\mathrm{out}}}\right) \times 100\%$$

$$\mathrm{CB}\ \text{conversion}(\%) = \frac{[\mathrm{CB}]_{\mathrm{in}} - [\mathrm{CB}]_{\mathrm{out}}}{[\mathrm{CB}]_{\mathrm{in}}} \times 100\%$$

$$\mathrm{CO}_2\ \text{selectivity}(\%) = \frac{[\mathrm{CO}_2]_{\mathrm{out}}}{6 \times ([\mathrm{CB}]_{\mathrm{in}} - [\mathrm{CB}]_{\mathrm{out}})} \times 100\%$$

where NO_x is the total concentration of NO and NO_2. $[NO]_{in}$, $[NO]_{out}$, $[N_2O]_{out}$, $[NO_x]_{in}$, $[NO_x]_{out}$, $[NH_3]_{in}$, and $[NH_3]_{out}$ indicates the corresponding inlet and outlet gas concentrations, respectively.

A more detailed description of the catalytic performance measurements is given in the SI.

2.3. Catalyst Characterizations. A detailed description of the further characterizations of the catalysts such as pyridine-infrared spectroscopy (Py-IR), temperature-programmed desorption of NH_3 (NH_3-TPD), and X-ray photoelectron spectroscopy (XPS) is given in the SI.

3. RESULTS AND DISCUSSION

3.1. Synergistic Abatement of NO_x and CB. The NO_x and CB conversions over MnO_2−$CePO_4/TiO_2$ catalysts with various Mn/Ce molar ratios were investigated. The sample with a Mn/Ce molar ratio of 4:6 showed the optimal performance of a broader active temperature window with over 80% NO_x and CB conversion and over 90% N_2 and CO_2 selectivity from 330 to 420 °C (Figure S1), which was selected for further experiments. Generally, in this temperature range, the VO_x/TiO_2 and V_2O_5−WO_3/TiO_2 catalysts showed approximately 50% CO_2 selectivity.[1,10] And the N_2 selectivity over the V_2O_5−MoO_3/TiO_2 and MnO_x−CeO_2 catalysts decreased severely.[5,13] The MnO_2−$CePO_4/TiO_2$ catalyst was expected to exhibit high NH_3-SCR and CBCO activity at the industrial application temperature of around 350 °C. For comparison, MnO_2/TiO_2 and $CePO_4/TiO_2$ catalysts were further investigated. The NO_x/CB conversion and N_2/CO_2 selectivity over the MnO_2−$CePO_4/TiO_2$ catalyst and reference catalysts are illustrated in Figure 1. The MnO_2/TiO_2 catalyst exhibited a NH_3-SCR temperature window of 240−390 °C with NO_x conversion above 80%, which did not match the CBCO degradation with conversion over 80% above 390 °C.

https://doi.org/10.1021/acs.est.1c08009
Environ. Sci. Technol. 2022, 56, 3719−3728

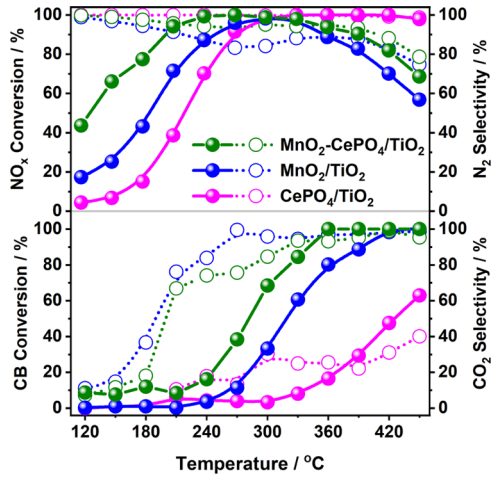

Figure 1. Plots of NO_x conversion (solid line), N_2 selectivity (dash line), CB conversion (solid line), and CO_2 selectivity (dash line) *versus* temperature over MnO_2−$CePO_4$/TiO_2, MnO_2/TiO_2, and $CePO_4$/TiO_2 catalysts. Reaction conditions: [NH_3] = [NO] = 500 ppm, [CB] = 100 ppm, [O_2] = 5 vol %, N_2 as balance gas, GHSV = 50 000 mL g^{-1} h^{-1}.

The N_2 selectivity was maintained around 85% within 240−420 °C, and the CO_2 selectivity was over 95% above 270 °C. The $CePO_4$/TiO_2 catalyst exhibited high activity on NH_3-SCR with NO_x conversion over 80% within 330−450 °C but a CB conversion less than 65% and a relatively low CO_2 selectivity less than 40% within 120−450 °C. The above results suggested that combining MnO_2 and $CePO_4$, the catalyst showed a synergistic performance of a broader active temperature window. For further understanding the roles of MnO_2 and $CePO_4$ in the synergistic conversion of NO_x and CB over MnO_2−$CePO_4$/TiO_2, the activities of MnO_2/TiO_2 C and $CePO_4$/TiO_2 C catalysts with MnO_2 (2 wt %) and $CePO_4$ (8 wt %) loadings as the same in MnO_2−$CePO_4$/TiO_2 (Mn/Ce ratio of 4:6) were tested (Figure S2). The MnO_2/TiO_2 C and $CePO_4$/TiO_2 C catalysts showed much worse CB conversions lower than 20 and 60% until 420 °C, respectively. It was further proved that MnO_2 and $CePO_4$ showed a synergistic effect on CB degradation while they were coupled. As for NO_x conversion, the activity of MnO_2−$CePO_4$/TiO_2 was enhanced below 270 °C but hampered above 330 °C mostly due to the strong redox ability of MnO_2, which also accounted for the production of N_2O and NO at higher temperatures. Furthermore, the addition of $CePO_4$ into V_2O_5−WO_3/TiO_2 could not improve the activity during the synergistic elimination of nitrogen oxides and chlorinated organics (Figure S3). It could be due to the insufficient redox ability of $CePO_4$, which could not compensate the defect of insufficient redox ability of V_2O_5−WO_3/TiO_2. On adding $CePO_4$ into MnO_2/TiO_2 directly, the MnO_2−$CePO_4$/TiO_2 would exhibit naturally stronger acidity and redox ability than MnO_2/TiO_2 C. Therefore, the MnO_2/TiO_2 and $CePO_4$/TiO_2 catalysts with 10% MnO_2 or $CePO_4$ loadings were selected as the comparison catalysts to reveal synergistic effects between MnO_2 and $CePO_4$ in further characterizations.

In the synergistic process of NH_3-SCR and CBCO, NH_3-SCR promoted the CB conversion (Figure S4). This could be ascribed to the NO_2 generated in the NH_3 oxidation or NO oxidation in the NH_3-SCR process (Figure S5) accelerating the reoxidation of reduced metallic oxide, which promoted the Mars and van Krevelen mechanism,[7,20] and both N_2 selectivity and CB conversion could be improved in this process. This was also reflected by that NO_2 concentration kept at nearly 0 ppm over the entire temperature range. The promoting effect of NO_2 was further confirmed by the temperature-programmed oxidation by NO_x/O_2-TPO) and NO_x + O_2-TPO after H_2 reduction (Figure S6). The oxidation peak of NO_x/O_2-TPO was broader from 240 to 270 °C, and the peak centered at 313.7 °C was at a lower temperature than the peak centered at 334.7 °C of O_2-TPO. It suggested the reduced MnO_2 or $CePO_4$ was easier to be oxidized into a higher valence state in the presence of NO_x, which evidenced that the NO_2 was able to accelerate the reoxidation of the catalysts. Further experiment showed that the CB conversion was suppressed by just the introduction of NH_3 and promoted by the introduction of NO (Figure S7). The promoting effect of NH_3-SCR on CBCO derived from the joint influence of NH_3 and NO_x. The *in situ* diffuse reflectance infrared Fourier transform (*in situ* DRIFT) spectra demonstrated that the peak at 1624 cm^{-1} originated from the adsorption of CB on Lewis acid sites was suppressed severely after the introduction of NH_3 (Figure S8).[21] It reflected that the competitive adsorption between NH_3 and CB on the acid sites occurred, which also accounted for the NO_x conversion decreasing due to CB addition at lower temperatures.[15] At this stage, few Lewis acid sites could be formed in the nucleophilic substitution to promote NH_3-SCR because the CB conversion was approximately 0 meanwhile. Above 300 °C, the CBCO reaction increased the NO_x conversion (Figure S4), and meanwhile the N_2 selectivity stopped decreasing and rebounded slightly. It could be correlated with the rapidly increased CB conversion above 210 °C (Figure S9). The CB oxidation consumed oxygen species and inhibited NH_3 oxidation, then the N_2O and NO formation was further inhibited.[6,7] Combining the NH_3 oxidation results (Figure S5), it could be further confirmed that the NH_3 overoxidation was suppressed in the synergistic reaction. As a result, the CBCO reaction suppressed the side reactions and promoted the NH_3-SCR performance at a high temperature range. Generally, over the MnO_2−$CePO_4$/TiO_2 catalyst, CBCO and NH_3-SCR showed synergistic improvement.

3.2. Structure and Composition. To better understand the enhancement of CBCO and NH_3-SCR over the MnO_2−$CePO_4$/TiO_2 catalyst, a series of structural and chemical properties of catalysts were investigated. X-ray diffraction (XRD) was applied to identify the crystal structure. The MnO_2−$CePO_4$/TiO_2 catalyst was composed of MnO_2 (JCPDS# 24-0735) and $CePO_4$ (JCPDS# 34-1380) loaded on TiO_2 (JCPDS# 21-1272) (Figure S10). Both phases loaded on TiO_2 corresponded well to the phases in MnO_2−$CePO_4$. And MnO_2 and $CePO_4$ were highly dispersed on TiO_2 according to the scanning electron microscope (SEM) images (Figure S11). XPS was utilized to further analyze the surface elemental composition and valence state. For accuracy, XPS was performed repeatedly, which showed similar results. The peaks of Mn $2p_{3/2}$ for MnO_2/TiO_2 and MnO_2−$CePO_4$/TiO_2 centered at 643.0, 642.0, 641.1 and 643.0, 641.4, 640.4 eV,[22] respectively (Figures S12A and 3A). The peaks of Ce $3d_{5/2}$ for $CePO_4$/TiO_2 and MnO_2−$CePO_4$/TiO_2 centered at 899.5, 886.7, 884.8, 881.9 and 900.2, 886.3, 884.5, 881.8 eV,[23] respectively (Figures S12B and 3B). Compared to MnO_2/TiO_2, $CePO_4$/TiO_2, the Mn 2p and Ce 3d peaks of MnO_2−$CePO_4$/TiO_2 shifting to lower binding energy revealed the

https://doi.org/10.1021/acs.est.1c08009
Environ. Sci. Technol. 2022, 56, 3719−3728

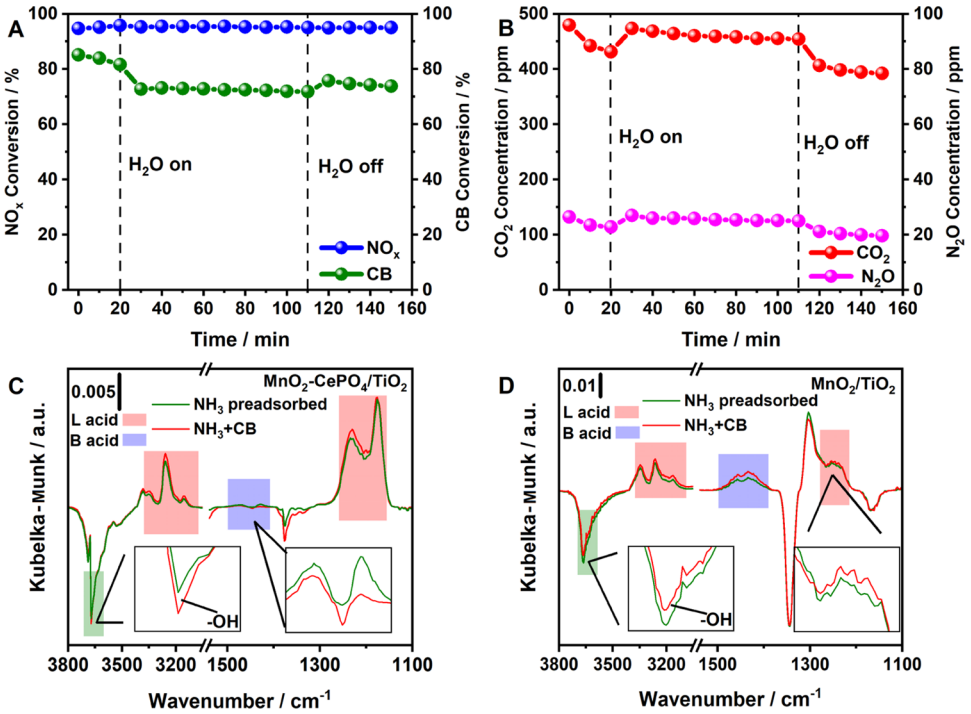

Figure 2. Plots of (A) NO_x and CB conversion, and (B) N_2 and CO_2 concentrations *versus* temperature over the MnO_2−$CePO_4/TiO_2$ catalyst in the presence of H_2O. Reaction conditions: 330 °C, [NH_3] = [NO] = 500 ppm, [CB] = 100 ppm, [O_2] = 5 vol %, N_2 as balance gas, [H_2O] = 6000 ppm (when used), GHSV = 50 000 mL g^{-1} h^{-1}; *in situ* DRIFT spectra of (C) the MnO_2−$CePO_4/TiO_2$ catalyst exposed to NH_3 + CB for 60 min after exposure to NH_3 for 60 min (saturated adsorption) at 210 °C and (D) the MnO_2/TiO_2 catalyst exposed to NH_3 + CB for 30 min after exposure to NH_3 for 120 min (saturated adsorption) at 210 °C. The inserted images were enlargements of the target areas.

interaction between Mn and Ce. The Ce^{4+}/Ce_{total} ratio increased from 48.7 to 64.8% and Mn^{4+}/Mn_{total} decreased from 44.0 to 42.9% (Table S1). The O 1s peaks (Figure S13) centered at approximately 529.8 eV were assigned to the lattice oxygen (O_{latt}), and the O 1s peaks centered at approximately 531.4 eV were attributed to chemisorbed oxygen (O_{ads}).[1] The amount of O_{ads} is in the order of MnO_2/TiO_2 > MnO_2−$CePO_4/TiO_2$ > $CePO_4/TiO_2$, which reflected the MnO_2−$CePO_4/TiO_2$ owned moderate redox ability. In addition, the XPS peaks of P 2p for both $CePO_4/TiO_2$ and MnO_2−$CePO_4/TiO_2$ centered at 132.9 and 133.9 eV, respectively (Figure S14).[24] Considering that the diffraction peak of $MnPO_4$ was not detected in the XRD pattern and the location of P 2p in XPS spectra was barely influenced by the addition of MnO_2, it could be deduced that P atoms did not interact with MnO_2 directly or the interaction was weak. Additionally, as the BET results suggested (Table S1), $CePO_4$ contributed more surface area than MnO_2 in MnO_2−$CePO_4/TiO_2$.

3.3. Redox and Acidity Properties. Both NH_3-SCR and CBCO reactions are based on acid and redox centers. To understand the enhanced synergistic mechanism of the MnO_2−$CePO_4/TiO_2$ catalyst, two important properties were further studied. On the one hand, the redox ability was evaluated using temperature-programmed reduction by H_2 (H_2-TPR) (Figure S15). For MnO_2/TiO_2, strong reduction peaks were located at 354 and 500 °C. The peak of $CePO_4/TiO_2$ centered at approximately 589 °C, which was much higher than that of MnO_2/TiO_2. It suggested the weak redox ability of $CePO_4/TiO_2$, which accounted for the low CB conversion and CO_2 selectivity for the CBCO reaction. Comparatively, MnO_2−$CePO_4/TiO_2$ exhibited H_2 consumption peaks at temperatures higher than MnO_2/TiO_2 and lower than $CePO_4/TiO_2$, and the intensities were much weaker than that of MnO_2/TiO_2. Totally, the redox ability of MnO_2−$CePO_4/TiO_2$ was stronger than $CePO_4/TiO_2$ but weaker than MnO_2/TiO_2, which was corresponded with the above XPS results. The moderate redox property enabled MnO_2−$CePO_4/TiO_2$ to oxidize CB into CO_2 and limited the formation of NO and N_2O in the NH_3-SCR.

On the other hand, the acid properties were investigated by NH_3-TPD, Py-IR, and NH_3 adsorption−desorption DRIFT spectra. In the NH_3-TPD profiles (Figure S16), the whole range was divided into three regions including weak acidity below 200 °C, moderate acidity from 200 to 350 °C, and strong acidity above 350 °C.[1] MnO_2−$CePO_4/TiO_2$ showed weaker acidity than MnO_2/TiO_2 in the temperature range of 50−350 °C but stronger acidity in the range of 350−450 °C provided by $CePO_4/TiO_2$. The Py-IR (Figure S17) was used to characterize the type of acid sites. The peaks at 1640 and 1542 cm^{-1} originated from Py adsorption on Brønsted acid sites, the bands at 1603, 1576, and 1445 cm^{-1} represent the Py adsorption on Lewis acid sites.[25,26] The MnO_2/TiO_2 showed a much higher Brønsted acid ratio than $CePO_4/TiO_2$ and MnO_2−$CePO_4/TiO_2$ (Table S2). Over the MnO_2−$CePO_4/TiO_2$ catalyst, the area ratio of total Brønsted acid to Lewis acid was decreased to 0.145 from 0.289 as the $CePO_4$ was introduced into MnO_2/TiO_2 system. Combining the result of NH_3-TPD, it could be deduced that the addition of $CePO_4$ provided abundant strong Lewis acid sites. This was further evidenced by the NH_3 adsorption−desorption DRIFT spectra (Figure S18). The MnO_2/TiO_2 catalyst exhibited stronger Brønsted acidity and more Brønsted acid sites than $CePO_4/TiO_2$ over 100 °C. Herein, Brønsted acid sites could be mainly ascribed to MnO_2. The bands appearing at 1601, 1185, and

https://doi.org/10.1021/acs.est.1c08009
Environ. Sci. Technol. 2022, 56, 3719−3728

1236 cm^{-1} over MnO_2−$CePO_4/TiO_2$ were assigned to Lewis acid sites, which were greatly enhanced compared to the bands over MnO_2/TiO_2 at 1602 and 1240 cm^{-1}.[27,28] Also, with increasing temperature, MnO_2−$CePO_4/TiO_2$ exhibited stronger Lewis acid than MnO_2/TiO_2 as NH_3-TPD demonstrated. Conversely, the bands at approximately 1434 cm^{-1} for MnO_2−$CePO_4/TiO_2$ assigned to Brønsted acid sites were weaker.[29] Over the $CePO_4/TiO_2$ catalyst, the bands that originated from NH_3 adsorption on the Lewis acid sites were still strong above 300 °C. It reflected that the introduction of $CePO_4$ brought strong Lewis acid sites into the MnO_2−$CePO_4/TiO_2$ catalyst. It could be reasonably speculated that the Lewis acid sites from $CePO_4$ played an important role in CB degradation.

Relating to catalyst performance, the insufficient redox ability could not oxidize the intermediates thoroughly in the CB degradation. MnO_2 provided sufficient redox ability to accomplish the CBCO reaction and would oxidize part of NH_3 into N_2O and NO_2 at high temperatures. As Figure S15 illustrates, the redox ability of MnO_2−$CePO_4/TiO_2$ was weaker than that of MnO_2/TiO_2 but stronger than that of $CePO_4/TiO_2$. However, with the assistance of $CePO_4$, which exhibited much weaker redox ability, the active temperature window of the synergistic reaction was lowered to prevent low N_2 selectivity. Meanwhile, the decomposition of CB suppressed the overoxidation of NH_3. Therefore, the high N_2 and CO_2 selectivity was maintained under high NO_x and CB conversion.

3.4. NH_3, CB, and H_2O Adsorption Behavior over Acid Sites. It has been realized that both NH_3 and chlorinated volatile organic compounds could adsorb on Lewis and Brønsted acid sites,[21,30] and H_2O could form complex with Lewis acid sites or convert Lewis acid sites into Brønsted acid sites.[31,32] Hence, the competitive adsorption behaviors of NH_3, CB, and H_2O on the acid sites during the reactions were observed. In Figure 2A, as 6000 ppm H_2O was introduced at 330 °C, the CB conversion dropped from 83 to 73%, and the NO_x conversion barely decreased meanwhile. Then, the CB conversion maintained around 73% and NO_x conversion slightly increased in the next 90 min until the H_2O was stopped. After the H_2O was stopped, the CB conversion recovered to 76% with NO_x conversion unchanged. There were two possibilities for the decrease of CB conversion. One was that the acid sites for CB adsorption were occupied, and the other one was that the oxidation step in the CB conversion process was suppressed.[33] Considering that the CO_2 and N_2O concentrations increased with the addition of H_2O (Figure 2B), it could be speculated that the oxidation process was not suppressed. Therefore, the suppression of CB adsorption on acid sites was most probably accounted for the decreased CB conversion.[6] To verify the speculation, *in situ* DRIFT spectra of CB + H_2O adsorption over MnO_2−$CePO_4/TiO_2$ were recorded (Figure S19). When H_2O was introduced into the CBCO reaction, the strengthening band at 1621 cm^{-1} attributed to H_2O overlapped the band at 1624 cm^{-1} assigned to CB adsorption on Lewis acid sites;[1,34] meanwhile, the band at 1641 cm^{-1} assigned to CB adsorption on Brønsted acid sites intensified.[35] In addition, as H_2O was introduced, *in situ* DRIFT spectra of NH_3 + H_2O (Figure S20) also reflected the bands from 1500 to 1400 cm^{-1} assigned to NH_3 adsorption on Brønsted acid sites intensified, which could be converted from the consumption of Lewis acid sites at 1224 cm^{-1}.[36] It indicated that the total adsorption of CB was not inhibited under the influence of the H_2O. More importantly, the converted Lewis acid sites played an important role in the promoted CBCO reaction. Although Brønsted acid sites were formed, which could be new sites for CB adsorption, actually it could not activate CB molecules as the original Lewis acid sites did. Therefore, the CB conversion was inhibited due to the suppressed CB adsorption on the strong Lewis acid sites with H_2O addition. At 300 °C, the deactivation was much more severe and the CB conversion dropped from 76% to approximately 50% (Figure S21), which showed the worse inhibition effect of H_2O on the CBCO reaction and revealed the significance of the strong Lewis acid sites on CB degradation at lower temperatures. However, for NH_3-SCR, the newly formed Brønsted acid sites were able to store more NH_3 to react with nitrates, which might be the reason for the slight NO conversion enhancement at higher temperatures. Then, the critical role of strong Lewis acid sites for promoting CB conversion was further studied in detail.

In situ DRIFTs of NH_3 and CB competitive adsorption at 210 °C were conducted over MnO_2/TiO_2, $CePO_4/TiO_2$, and MnO_2−$CePO_4/TiO_2$. The adsorption of each gas atmosphere was not switched or stopped until it was saturated. For MnO_2−$CePO_4/TiO_2$ (Figure 2C), when the CB was introduced after saturated adsorption of NH_3, intensification of bands corresponded to NH_3 adsorbed on Lewis acid sites at 3383, 3346, 3260, 3156, and 1230 cm^{-1} occurred as the bands assigned to NH_3 adsorbed on Brønsted acid sites weakened (1500−1400 cm^{-1}).[37] This could be due to the nucleophilic substitution between CB and Brønsted acid led to the consumption of Brønsted acid and formation of new Lewis acid sites. The consumption of the −OH species at 3672 cm^{-1} further confirmed this.[1] In contrast, for MnO_2/TiO_2 (Figure 2D), the Lewis acid sites also increased as the CB was introduced.[38] However, the bands assigned to Brønsted acid sites intensified accompanied with the −OH species partly recovering. The intensification could be due to newly formed Brønsted acid sites or the competitive adsorption of CB on the Brønsted acid sites, which released hydroxyl groups from the combination with NH_3.[11,18,19,39] Over MnO_2−$CePO_4/TiO_2$, this effect was covered by the consumed Brønsted acid. For the $CePO_4/TiO_2$ catalyst (Figure S22), as the CB was introduced, the bands from 1500 to 1400 cm^{-1} corresponded to the NH_3 adsorption on Brønsted acid sites weakened due to Brønsted acid being consumed or occupied by CB, and the −OH species (bands around 3600 cm^{-1}) were consumed through nucleophilic substitution. The signal of NH_3 adsorption on Lewis acid sites (1233 and 1184 cm^{-1}) weakened due to the competitive adsorption of CB, and the newly formed Lewis acid sites were not observed because of the low content of Brønsted acid over $CePO_4/TiO_2$. These phenomena indicated that the MnO_2−$CePO_4/TiO_2$ catalyst possessed higher activity in the nucleophilic substitution process, over which the consumption of Brønsted acid (−OH species) and the formation of phenolate species were promoted. To further understand how $CePO_4$ affected the nucleophilic substitution process, the *in situ* Raman spectra of MnO_2−$CePO_4/TiO_2$ exposed to CB at 50 °C were recorded (Figure S23). After CB adsorption over MnO_2−$CePO_4/TiO_2$, the Raman bands at approximately 465.5 and 971.6 cm^{-1} attributed to the P−O bonds in $CePO_4$ shifted to 456.7 and 968.3 cm^{-1}, respectively.[40] And the bands at 650.2 cm^{-1} attributed to the Mn−O stretching vibration was not affected.[41] The redshift over $CePO_4$ indicated that $CePO_4$ was charge-compensated by adsorbed CB. Considering that the Cl could adsorb on the

https://doi.org/10.1021/acs.est.1c08009
Environ. Sci. Technol. 2022, 56, 3719−3728

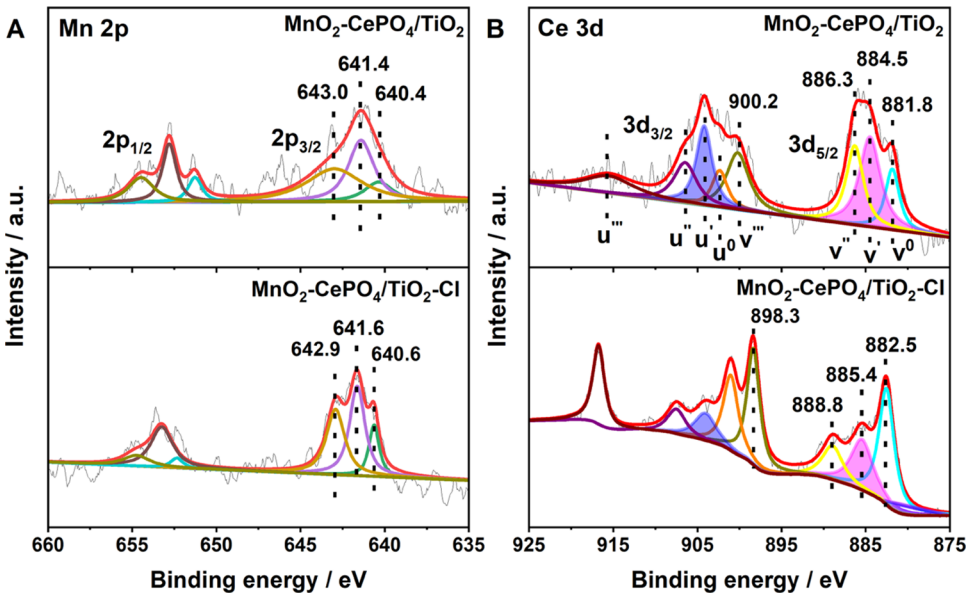

Figure 3. XPS spectra of (A) Mn 2p and (B) Ce 3d for MnO_2−$CePO_4/TiO_2$ and MnO_2−$CePO_4/TiO_2$-Cl catalysts.

Lewis acid sites,[42] it could be speculated that the electron cloud density of adsorbed CB and the C−Cl bond were weakened.[43] In addition, the redshift of the bands attributed to $CePO_4$ and MnO_2 over MnO_2−$CePO_4$ also suggested the combination and interaction of MnO_2 and $CePO_4$. It could be concluded that the addition of $CePO_4$ provided abundant strong Lewis acid sites, which were able to weaken the electron cloud density between Cl and benzene ring when the CB molecules were attacked by Brønsted acid. In this way, the C−Cl bond was weakened and the dechlorination was promoted accompanied with CB being easier to be attacked by −OH over MnO_2. In the followed steps, MnO_2 offered sufficient oxidizability to further oxidize the phenolates into CO_2 and H_2O. This strategy was found to be also effective for other catalysts. The γ-Al_2O_3 is known as a support possessing abundant strong Lewis acid sites.[44] We constructed MnO_2/γ-Al_2O_3 and MnO_2/TiO_2 with 5 wt % MnO_2, where the former also showed decreased CB conversion temperature compared to the latter (Figure S24).

3.5. Poisoning and Deactivation Analyses. Cl poisoning on catalysts was found to hamper the catalytic activities, and the dissociated Cl could bond with metallic oxides and deactivate the active sites.[17,33] After the NH_3-SCR and CBCO synergistic reaction, MnO_2−$CePO_4/TiO_2$ showed XPS peaks of Cl 2p centered at 198.0 and 199.7 eV (Figure S25). The surface area of MnO_2−$CePO_4/TiO_2$ sightly decreased (Table S1). And the redox ability of the MnO_2−$CePO_4/TiO_2$ catalyst was found to be weakened as the H_2-TPR peaks shifted approximately 20 °C to higher temperatures (Figure S15). As a result, with decreasing CB conversion, the NO_x conversion and N_2 selectivity were improved as the synergistic reaction proceeded at 360 °C (Figure S26). In addition, NH_3-TPD (Figure S16) showed that MnO_2−$CePO_4/TiO_2$-Cl possessed stronger acidity after Cl poisoning. The deposition of Cl on the catalyst, which would lead to the formation of NH_4Cl, provided extra Brønsted acid sites.[11] However, NH_4Cl had been proved to decompose effectively at approximately 200 °C over the V_2O_5−WO_3/TiO_2 catalyst.[45] Therefore, the stronger acidity could be due to the combination of Cl and metallic oxides. The Cl as an electron-withdrawing group might enhance the electrophilicity of the metal sites. Thereby, these metal sites combined with −OH to form Brønsted acid sites.[39] The area ratio of Brønsted acid sites to Lewis acid sites calculated from Py-IR increased from 0.141 to 0.231 after Cl poisoning (Figure S17 and Table S2). This could also explain the intensification of bands from 1500 to 1400 cm^{-1} (NH_3 adsorption on Brønsted acid sites) and recovered −OH species when CB was introduced (Figure 2D). To further understand the effects of the Cl poisoning on the MnO_2−$CePO_4/TiO_2$ catalyst, XPS of MnO_2−$CePO_4/TiO_2$-Cl was conducted (Figure 3). Compared to MnO_2−$CePO_4/TiO_2$, the XPS characteristic peaks of Ce 3d and Mn 2p shifted to higher binding energies, indicating the combination of Cl with Mn and Ce.[46] Thus, the ratio of Ce^{4+} to Ce_{total} increased from 64.8 to 80.3% and the ratio of Mn^{4+} to Mn_{total} decreased from 42.9 to 33.8% (Table S1), indicating that the Ce suffered heavier Cl poisoning than Mn did, and the MnO_2 as the dominated redox site was reduced during the reaction.[47] Meanwhile, the proportion of O_{ads} decreased from 25.5 to 22.4% (Figure S13). It was noted that the existence of H_2O alleviated the Cl poisoning over the MnO_2−$CePO_4/TiO_2$ catalyst (Figure 2A), although the H_2O decreased the CB conversion by inhibiting the adsorption of CB on strong Lewis acid sites. In the first 20 min, the CB conversion decreased from 85 to 83%. In the presence of H_2O, the CB conversion slightly decreased from 73 to 72% during 90 min but decreased from 76 to 74% during 30 min since H_2O was cut off. It was found that H_2O could remove the chloride and coke on the catalysts by forming extra hydroxyl and promoting the generation of HCl.[17,18,46] The residual carbon was analyzed by thermal gravity (TG). The MnO_2−$CePO_4/TiO_2$-Cl catalyst only exhibited a 0.07% mass difference from the fresh MnO_2−$CePO_4/TiO_2$ catalyst (Figure S27), which suggested that the impact of carbon deposition was quite limited. In conclusion, the Cl poisoning to the MnO_2−$CePO_4/TiO_2$ catalyst decreased the surface area (Table S1), weakened the redox ability, and changed the acid properties of metal sites. The Cl preferred to combine with Ce Lewis acid sites and increased the Ce(IV) proportion. Nonetheless, Cl poisoning increased N_2 selectivity at higher

https://doi.org/10.1021/acs.est.1c08009
Environ. Sci. Technol. 2022, 56, 3719−3728

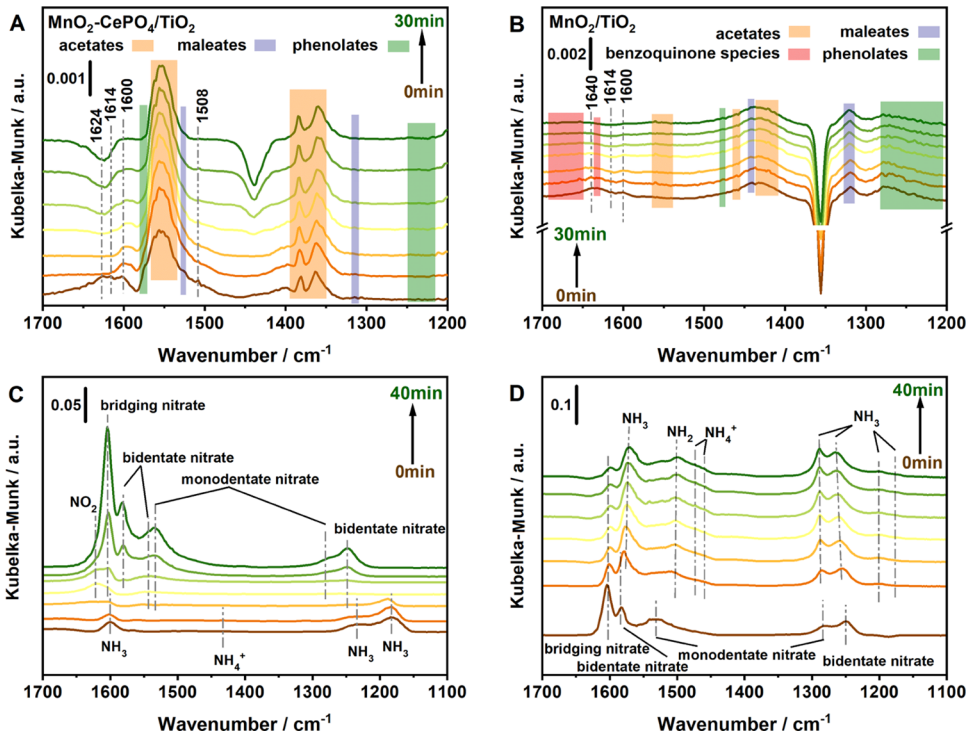

Figure 4. *In situ* DRIFT spectra of the transient reactions between O_2 and preadsorbed CB over (A) MnO_2−$CePO_4/TiO_2$ and (B) MnO_2/TiO_2 catalysts at 210 °C. (C) *In situ* DRIFT spectra of the transient reactions between NO + O_2 and preadsorbed NH_3 over the MnO_2−$CePO_4/TiO_2$ catalyst. (D) *In situ* DRIFT spectra of the transient reactions between NH_3 and preadsorbed NO + O_2 over the MnO_2−$CePO_4/TiO_2$ catalyst.

temperatures and the newly formed Brønsted acid sites could provide additional active sites for NH_3-SCR.

3.6. Reaction Mechanism. To further get insights into the synergistic mechanism of CBCO and NH_3-SCR over MnO_2−$CePO_4/TiO_2$, $CePO_4/TiO_2$, and MnO_2/TiO_2 catalysts, *in situ* DRIFT measurements were performed. Over MnO_2−$CePO_4/TiO_2$ (Figure 4A), the CB initially adsorbed on Lewis acid sites (1624 and 1614 cm^{-1}) with the band at 1508 cm^{-1} originated from the adsorbed benzene ring.[1,21,48] Then, the adsorbed CB molecules were consumed by the attack of Brønsted acid over MnO_2 within 15 min. The bands of phenolates (1575, 1244, and 1217 cm^{-1}) and catecholates (1600 cm^{-1}) remained unchanged for the first 4 min.[21,49] Then, with the oxidation of phenolates and catecholates by Mn−O−Mn, more acetates (1562, 1557, 1552, 1545, 1535, 1381, and 1361 cm^{-1}) were accumulated in the first 25 min and then to be consumed (Figure S28),[1,21,50] and the maleates (1525 and 1314 cm^{-1}) were consumed from the beginning.[49−51] Over the $CePO_4/TiO_2$ catalyst (Figure S29), the oxidation process did not take place as fast as over the MnO_2−$CePO_4/TiO_2$ catalyst. As O_2 was added, the phenolates (1572 and 1219 cm^{-1}) increased and accumulated in the first 10 min. The maleates (1527 and 1521 cm^{-1}) went through an enhancement process before reduction,[1,49] and the amount of acetates (1559, 1553, 1547, 1537, 1384, 1373, 1361, and 1350 cm^{-1}) increased during the whole 30 min.[1,21,52] It reflected that over $CePO_4/TiO_2$, the intermediates could not be oxidized efficiently due to the insufficiency of redox ability, but it could convert the CB into phenolates effectively, which confirmed that the Lewis acid sites promoted the nucleophilic substitution process. Over the MnO_2/TiO_2 catalyst (Figure 4B), the adsorbed CB (1614 cm^{-1}) on Lewis acid sites and on Brønsted acid sites (1640 cm^{-1}),[13,35] with phenolates (1477 cm^{-1} and bands from 1200 to 1300 cm^{-1}) and catecholates (1600 cm^{-1}) were not completely consumed during 30 min. Then, the maleates (1442 and 1320 cm^{-1}) and acetates (1560, 1541, 1460, 1431, 1420, and 1414 cm^{-1}) remained at relatively steady levels,[21,49,51] which suggested that the nucleophilic substitution process did not proceed effectively, and the deeper oxidation of phenolates and catecholates into maleates and acetates reached a balance. Besides, benzoquinone species (1686, 1676, 1655, and 1631 cm^{-1}) were also presented over the MnO_2/TiO_2 catalyst.[1,34,52,53] As a result, MnO_2/TiO_2 showed weaker activity of CB conversion into nucleophilic substitution products at 210 °C. Generally, MnO_2−$CePO_4/TiO_2$-integrated $CePO_4$ and MnO_2 showed high activity on both nucleophilic substitution process and the following deeper oxidation process. The strong Lewis acid sites mainly supplied by $CePO_4$ induced CB conversion under a lower temperature, which better matched the NH_3-SCR temperature window.

The NH_3-SCR was then analyzed over MnO_2−$CePO_4/TiO_2$. As the NO was introduced after the preadsorption of NH_3 (Figure 4C), the NH_3 molecules adsorbed on Lewis acid sites (1601, 1234, and 1184 cm^{-1}) were first consumed and then NH_4^+ on Brønsted acid sites (1433 cm^{-1}) were consumed after 5 min.[29] The bands assigned to NO_2 (1622 cm^{-1}), bridging nitrates (1604 cm^{-1}), bidentate nitrates (1581, 1543, and 1248 cm^{-1}), and monodentate nitrates (1533 and 1281 cm^{-1}) appeared when NH_3 and NH_4^+ were completely consumed,[29,54,55] indicating that the NH_3 adsorbed on Lewis acid sites preferentially reacted with the nitrates. After the preadsorption of NO + O_2 (Figure 4D), bridging nitrates (1603 cm^{-1}), bidentate nitrates (1583 and 1250 cm^{-1}), and monodentate nitrates (1531 and 1286 cm^{-1}) appeared. When bidentate nitrates and monodentate nitrates were completely consumed, NH_3 (1572, 1289, 1263, 1201, and 1176 cm^{-1}),

https://doi.org/10.1021/acs.est.1c08009
Environ. Sci. Technol. 2022, 56, 3719−3728

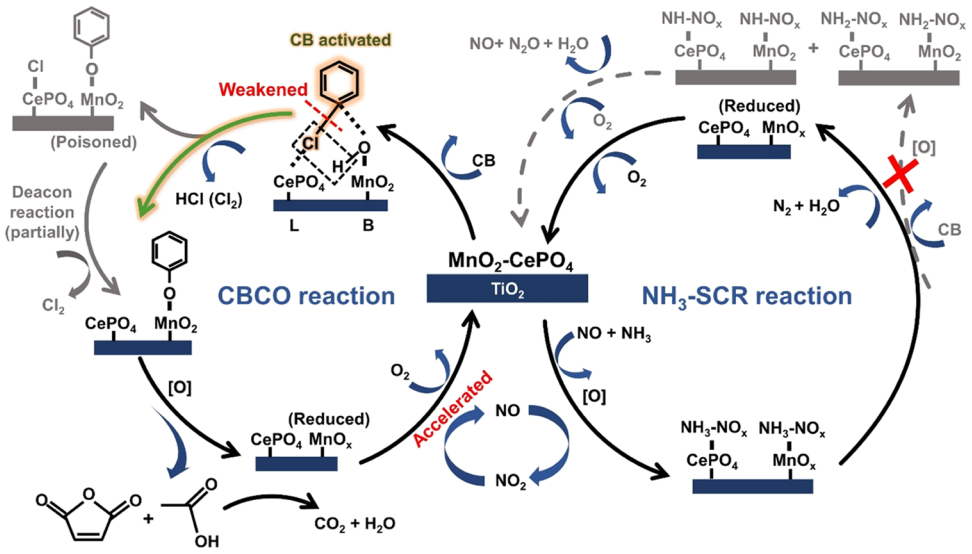

Figure 5. Schematic illustration of the synergistic catalytic removal of NO_x and CB over MnO_2−$CePO_4$/TiO_2 catalysts.

NH_2 (1500 cm^{-1}), and NH_4^+ (1473 and 1460 cm^{-1}) were observed. However, the bridging nitrates (1600 cm^{-1}) were consumed slowly.[29,54−56] Therefore, the NH_3-SCR over the MnO_2−$CePO_4$/TiO_2 catalyst followed the Langmuir−Hinshelwood mechanism.[6]

Here, we proposed a reaction pathway for the CBCO and NH_3-SCR synergistic reaction over the MnO_2−$CePO_4$/TiO_2 catalyst (Figure 5). Both reactions were based on the acid cycle and the redox cycle. For the CBCO reaction, the CB adsorbed on $CePO_4$ (Lewis acid sites) and the bond between Cl and benzene ring was weakened by the electronic traction of $CePO_4$, thereby the carbon site connected with Cl was easier to be attacked by the hydroxyl groups (Brønsted acid sites) on MnO_2. Then, the nucleophilic substitution occurred accompanied with the removal of Cl with H and the formation of phenolates. Then, the phenolates formed over MnO_2 were oxidized into acetates and maleates and then further oxidized into CO_2 and H_2O. The reduced Mn(II, III) species were reoxidized by O_2 into higher valence Mn(III, IV), and this step was accelerated by NO_2 originated from the synergistic NH_3-SCR process. The Ce sites could be poisoned by Cl and oxidized into higher valence Ce(IV), and parts of the Cl deposited over Ce sites could be removed through the Deacon reaction.[16] For the NH_3-SCR, the NH_3 and NO were initially adsorbed on Lewis acid sites over MnO_2 and $CePO_4$. Subsequently, the NH_3-NO_x species were formed, ultimately decomposing into N_2 and H_2O. NH_3-SCR side reactions were inhibited, which benefited from the strong oxidative species consumed by the CBCO and prevented the deeper oxidation of NH_3 to NH_2 or NH that led to the formation of N_2O and NO.[7]

■ ASSOCIATED CONTENT

Supporting Information

The Supporting Information is available free of charge at https://pubs.acs.org/doi/10.1021/acs.est.1c08009.

Characterization of catalysts; catalytic performance tests; NH_3-SCR and CBCO activities (Figures S1, S2, S3, S4, S5, S7, S9, and S24), O_2-TPO and NO_x/O_2-TPO (Figure S6); *in situ* DRIFT spectra (Figures S8, S18, S19, S20, S22, S28, and S29); XRD patterns (Figure S10); SEM (Figure S11); XPS (Figures S12, S13, S14, and S25, and Table S1); specific surface area (Table S1); H_2-TPR (Figure S15); NH_3-TPD (Figure S16); Py-IR (Figure S17 and Table S2); H_2O-resistant test (Figure S21); Raman spectra (Figure S23); catalytic stability (Figure S26); and TG (Figure S27) (PDF)

■ AUTHOR INFORMATION

Corresponding Authors

Aling Chen − *International Joint Laboratory of Catalytic Chemistry, State Key Laboratory of Advanced Special Steel, Department of Chemistry, Research Center of Nano Science and Technology, College of Sciences, Shanghai University, Shanghai 200444, P. R. China*; Phone: +86-21-66137152; Email: chenalingshuo@shu.edu.cn

Dengsong Zhang − *International Joint Laboratory of Catalytic Chemistry, State Key Laboratory of Advanced Special Steel, Department of Chemistry, Research Center of Nano Science and Technology, College of Sciences, Shanghai University, Shanghai 200444, P. R. China*; orcid.org/0000-0003-4280-0068; Phone: +86-21-66137152; Email: dszhang@shu.edu.cn

Authors

Chi Zhang − *International Joint Laboratory of Catalytic Chemistry, State Key Laboratory of Advanced Special Steel, Department of Chemistry, Research Center of Nano Science and Technology, College of Sciences, Shanghai University, Shanghai 200444, P. R. China*

Jianping Zhang − *International Joint Laboratory of Catalytic Chemistry, State Key Laboratory of Advanced Special Steel, Department of Chemistry, Research Center of Nano Science and Technology, College of Sciences, Shanghai University, Shanghai 200444, P. R. China*

Yongjie Shen − *International Joint Laboratory of Catalytic Chemistry, State Key Laboratory of Advanced Special Steel, Department of Chemistry, Research Center of Nano Science and Technology, College of Sciences, Shanghai University, Shanghai 200444, P. R. China*

Jiebing He − *International Joint Laboratory of Catalytic Chemistry, State Key Laboratory of Advanced Special Steel, Department of Chemistry, Research Center of Nano Science*

https://doi.org/10.1021/acs.est.1c08009
Environ. Sci. Technol. 2022, 56, 3719−3728

and Technology, College of Sciences, Shanghai University, Shanghai 200444, P. R. China

Wenqiang Qu − *International Joint Laboratory of Catalytic Chemistry, State Key Laboratory of Advanced Special Steel, Department of Chemistry, Research Center of Nano Science and Technology, College of Sciences, Shanghai University, Shanghai 200444, P. R. China*

Jiang Deng − *International Joint Laboratory of Catalytic Chemistry, State Key Laboratory of Advanced Special Steel, Department of Chemistry, Research Center of Nano Science and Technology, College of Sciences, Shanghai University, Shanghai 200444, P. R. China*

Lupeng Han − *International Joint Laboratory of Catalytic Chemistry, State Key Laboratory of Advanced Special Steel, Department of Chemistry, Research Center of Nano Science and Technology, College of Sciences, Shanghai University, Shanghai 200444, P. R. China*

Complete contact information is available at: https://pubs.acs.org/10.1021/acs.est.1c08009

Notes

The authors declare no competing financial interest.

■ ACKNOWLEDGMENTS

The authors acknowledge the support of the National Key R&D Program of China (2017YFE0132400) and the National Natural Science Foundation of China (22125604).

■ REFERENCES

(1) Long, Y.; Su, Y.; Xue, Y.; Wu, Z.; Weng, X. V_2O_5-WO_3/TiO_2 catalyst for efficient synergistic control of NO_x and chlorinated organics: Insights into the arsenic effect. *Environ. Sci. Technol.* **2021**, *55*, 9317−9325.

(2) He, C.; Cheng, J.; Zhang, X.; Douthwaite, M.; Pattisson, S.; Hao, Z. Recent advances in the catalytic oxidation of volatile organic compounds: A review based on pollutant sorts and sources. *Chem. Rev.* **2019**, *119*, 4471−4568.

(3) Ou, J.; Yuan, Z.; Zheng, J.; Huang, Z.; Shao, M.; Li, Z.; Huang, X.; Guo, H.; Louie, P. K. K. Ambient ozone control in a photochemically active region: Short-term despiking or long-term attainment? *Environ. Sci. Technol.* **2016**, *50*, 5720−5728.

(4) Marberger, A.; Ferri, D.; Elsener, M.; Krocher, O. The significance of Lewis acid sites for the selective catalytic reduction of nitric oxide on vanadium-based catalysts. *Angew. Chem., Int. Ed.* **2016**, *55*, 11989−11994.

(5) Gan, L.; Li, K.; Xiong, S.; Zhang, Y.; Chen, J.; Peng, Y.; Li, J. MnO_x-CeO_2 catalysts for effective NO_x reduction in the presence of chlorobenzene. *Catal. Commun.* **2018**, *117*, 1−4.

(6) Han, L.; Cai, S.; Gao, M.; Hasegawa, J. Y.; Wang, P.; Zhang, J.; Shi, L.; Zhang, D. Selective catalytic reduction of NO_x with NH_3 by using novel catalysts: State of the art and future prospects. *Chem. Rev.* **2019**, *119*, 10916−10976.

(7) Gan, L.; Shi, W.; Li, K.; Chen, J.; Peng, Y.; Li, J. Synergistic promotion effect between NO_x and chlorobenzene removal on MnO_x-CeO_2 catalyst. *ACS Appl. Mater. Interfaces* **2018**, *10*, 30426−30432.

(8) Gallastegi-Villa, M.; Aranzabal, A.; González-Marcos, J. A.; González-Velasco, J. R. Metal-loaded ZSM5 zeolites for catalytic purification of dioxin/furans and NO_x containing exhaust gases from MWI plants: Effect of different metal cations. *Appl. Catal., B* **2016**, *184*, 238−245.

(9) Milligan, M. S.; Altwicker, E. The relationship between de novo synthesis of polychlorinated dibenzo-p-dioxins and dibenzofurans and low-temperature carbon gasification in fly ash. *Environ. Sci. Technol.* **1993**, *27*, 1595−1601.

(10) Zhai, S.; Su, Y.; Weng, X.; Li, R.; Wang, H.; Wu, Z. Synergistic elimination of NO_x and chlorinated organics over VO_x/TiO_2 catalysts: A combined experimental and DFT study for exploring vanadate domain effect. *Environ. Sci. Technol.* **2021**, *55*, 12862−12870.

(11) Wang, D.; Chen, J.; Peng, Y.; Si, W.; Li, X.; Li, B.; Li, J. Dechlorination of chlorobenzene on vanadium-based catalysts for low-temperature SCR. *Chem. Commun.* **2018**, *54*, 2032−2035.

(12) Li, G.; Shen, K.; Wu, P.; Zhang, Y.; Hu, Y.; Xiao, R.; Wang, B.; Zhang, S. SO_2 poisoning mechanism of the multi-active center catalyst for chlorobenzene and NO_x synergistic degradation at dry and humid environments. *Environ. Sci. Technol.* **2021**, *55*, 13186−13197.

(13) Huang, X.; Wang, D.; Yang, Q.; Peng, Y.; Li, J. Multi-pollutant control (MPC) of NO and chlorobenzene from industrial furnaces using a vanadia-based SCR catalyst. *Appl. Catal., B* **2021**, *285*, No. 119835.

(14) Wei, L.; Liu, Y.; Dai, H.; Cui, S.; Wang, C.; Hsi, H.-C.; Duan, E.; Peng, Y.; Deng, J. Electronic structure tailoring of Al^{3+}- and Ta^{5+}-doped CeO_2 for the synergistic removal of NO and chlorinated organics. *Appl. Catal., B* **2022**, *304*, No. 120939.

(15) Gan, L.; Wang, Y.; Chen, J.; Yan, T.; Li, J.; Crittenden, J.; Peng, Y. The synergistic mechanism of NO_x and chlorobenzene degradation in municipal solid waste incinerators. *Catal. Sci. Technol.* **2019**, *9*, 4286−4292.

(16) Dai, Q.; Bai, S.; Wang, X.; Lu, G. Catalytic combustion of chlorobenzene over Ru-doped ceria catalysts: Mechanism study. *Appl. Catal., B* **2013**, *129*, 580−588.

(17) Weng, X.; Meng, Q.; Liu, J.; Jiang, W.; Pattisson, S.; Wu, Z. Catalytic oxidation of chlorinated organics over lanthanide perovskites: Effects of phosphoric acid etching and water vapor on chlorine desorption behavior. *Environ. Sci. Technol.* **2019**, *53*, 884−893.

(18) Dai, X.; Wang, X.; Long, Y.; Pattisson, S.; Lu, Y.; Morgan, D. J.; Taylor, S. H.; Carter, J. H.; Hutchings, G. J.; Wu, Z.; Weng, X. Efficient elimination of chlorinated organics on a phosphoric acid modified CeO_2 catalyst: A hydrolytic destruction route. *Environ. Sci. Technol.* **2019**, *53*, 12697−12705.

(19) González-Velasco, J.; López-Fonseca, R.; Aranzabal, A.; Gutiérrez-Ortiz, J. I.; Steltenpohl, P. Evaluation of H-type zeolites in the destructive oxidation of chlorinated volatile organic compounds. *Appl. Catal., B* **2000**, *24*, 233−242.

(20) Li, G.; Shen, K.; Wang, L.; Zhang, Y.; Yang, H.; Wu, P.; Wang, B.; Zhang, S. Synergistic degradation mechanism of chlorobenzene and NO_x over the multi-active center catalyst: The role of NO_2, Brønsted acidic site, oxygen vacancy. *Appl. Catal., B* **2021**, *286*, No. 119865.

(21) Weng, X.; Xue, Y.; Chen, J.; Meng, Q.; Wu, Z. Elimination of chloroaromatic congeners on a commercial V_2O_5-WO_3/TiO_2 catalyst: The effect of heavy metal Pb. *J. Hazard. Mater.* **2020**, *387*, No. 121705.

(22) Tan, X.; Wan, Y.; Huang, Y.; He, C.; Zhang, Z.; He, Z.; Hu, L.; Zeng, J.; Shu, D. Three-dimensional MnO_2 porous hollow microspheres for enhanced activity as ozonation catalysts in degradation of bisphenol A. *J. Hazard. Mater.* **2017**, *321*, 162−172.

(23) Liu, S.; Liu, J.; Lin, Q.; Xu, S.; Wang, J.; Xu, H.; Chen, Y. Solvent effects on the low-temperature NH_3−SCR activity and hydrothermal stability of WO_3/SiO_2@$CeZrO_x$ catalyst. *ACS Sustainable Chem. Eng.* **2020**, *8*, 13418−13429.

(24) Li, J.; Zhang, W.; Ran, M.; Sun, Y.; Huang, H.; Dong, F. Synergistic integration of Bi metal and phosphate defects on hexagonal and monoclinic $BiPO_4$: Enhanced photocatalysis and reaction mechanism. *Appl. Catal., B* **2019**, *243*, 313−321.

(25) Zhang, P.; Wang, P.; Chen, A.; Han, L.; Yan, T.; Zhang, J.; Zhang, D. Alkali-resistant catalytic reduction of NO_x by using Ce-O-B alkali-capture sites. *Environ. Sci. Technol.* **2021**, *55*, 11970−11978.

(26) Cai, S.; Xu, T.; Wang, P.; Han, L.; Impeng, S.; Li, Y.; Yan, T.; Chen, G.; Shi, L.; Zhang, D. Self-protected CeO_2-SnO_2@SO_4^{2-}/TiO_2 catalysts with extraordinary resistance to alkali and heavy metals for NO_x reduction. *Environ. Sci. Technol.* **2020**, *54*, 12752−12760.

(27) Liu, Z.; Zhang, S.; Li, J.; Ma, L. Promoting effect of MoO_3 on the NO_x reduction by NH_3 over CeO_2/TiO_2 catalyst studied with in situ DRIFTS. *Appl. Catal., B* **2014**, *144*, 90−95.

(28) Smirniotis, P. G.; Peña, D. A.; Uphade, B. S. Low-temperature selective catalytic reduction (SCR) of NO with NH_3 by using Mn, Cr, and Cu oxides supported on hombikat TiO_2. *Angew. Chem., Int. Ed.* **2001**, *40*, 2479−2482.
(29) Ma, Z.; Wu, X.; Härelind, H.; Weng, D.; Wang, B.; Si, Z. NH_3-SCR reaction mechanisms of NbO_x /$Ce_{0.75}Zr_{0.25}O_2$ catalyst: DRIFTS and kinetics studies. *J. Mol. Catal. A: Chem.* **2016**, *423*, 172−180.
(30) Aristizábal, B. H.; de Correa, C. M.; Serykh, A. I.; Hetrick, C. E.; Amiridis, M. D. In situ FTIR study of the adsorption and reaction of ortho-dichlorobenzene over Pd-promoted Co-HMOR. *Microporous Mesoporous Mater.* **2008**, *112*, 432−440.
(31) Bolis, V.; Busco, C.; Ugliengo, P. Thermodynamic study of water adsorption in high-silica zeolites. *J. Phys. Chem. B* **2006**, *110*, 14849−14859.
(32) Cui, Z.; Feng, X.; Li, H.; Tan, T. Interconversion of Lewis acid and Brønsted acid catalysts in biomass-derived paraxylene synthesis. *Chem. Eng. Sci.* **2020**, *227*, No. 115942.
(33) Wang, D.; Chen, Q.; Zhang, X.; Gao, C.; Wang, B.; Huang, X.; Peng, Y.; Li, J.; Lu, C.; Crittenden, J. Multipollutant control (MPC) of flue gas from stationary sources using SCR technology: A critical review. *Environ. Sci. Technol.* **2021**, *55*, 2743−2766.
(34) Li, N.; Cheng, J.; Xing, X.; Sun, Y.; Hao, Z. Distribution and formation mechanisms of polychlorinated organic by-products upon the catalytic oxidation of 1,2-dichlorobenzene with palladium-loaded catalysts. *J. Hazard. Mater.* **2020**, *393*, No. 122412.
(35) Weng, X.; Sun, P.; Long, Y.; Meng, Q.; Wu, Z. Catalytic oxidation of chlorobenzene over $Mn_xCe_{1-x}O_2$/HZSM-5 catalysts: A study with practical implications. *Environ. Sci. Technol.* **2017**, *51*, 8057−8066.
(36) Huang, L.; Zha, K.; Namuangruk, S.; Junkaew, A.; Zhao, X.; Li, H.; Shi, L.; Zhang, D. Promotional effect of the TiO_2 (001) facet in the selective catalytic reduction of NO with NH_3: In situ DRIFTS and DFT studies. *Catal. Sci. Technol.* **2016**, *6*, 8516−8524.
(37) Chen, L.; Si, Z.; Wu, X.; Weng, D. DRIFT study of CuO-CeO_2-TiO_2 mixed oxides for NO_x reduction with NH_3 at low temperatures. *ACS Appl. Mater. Interfaces* **2014**, *6*, 8134−8145.
(38) Li, X.; Li, J.; Peng, Y.; Si, W.; He, X.; Hao, J. Regeneration of commercial SCR catalysts: Probing the existing forms of arsenic oxide. *Environ. Sci. Technol.* **2015**, *49*, 9971−9978.
(39) Tanaka, M.; Ogasawara, S. Infrared studies of the adsorption and the catalysis of hydrogen chloride on alumina and on silica. *J. Catal.* **1970**, *16*, 157−163.
(40) Asuvathraman, R.; Gnanasekar, K. I.; Clinsha, P. C.; Ravindran, T. R.; Kutty, K. V. G. Investigations on the charge compensation on Ca and U substitution in $CePO_4$ by using XPS, XRD and Raman spectroscopy. *Ceram. Int.* **2015**, *41*, 3731−3739.
(41) Liu, H.; Li, X.; Dai, Q.; Zhao, H.; Chai, G.; Guo, Y.; Guo, Y.; Wang, L.; Zhan, W. Catalytic oxidation of chlorinated volatile organic compounds over Mn-Ti composite oxides catalysts: Elucidating the influence of surface acidity. *Appl. Catal., B* **2021**, *282*, No. 119577.
(42) Du, C.; Lu, S.; Wang, Q.; Buekens, A. G.; Ni, M.; Debecker, D. P. A review on catalytic oxidation of chloroaromatics from flue gas. *Chem. Eng. J.* **2018**, *334*, 519−544.
(43) Godiksen, A. L.; Rasmussen, S. B. Identifying the presence of $[V{=}O]^{2+}$ during SCR using in-situ Raman and UV Vis spectroscopy. *Catal. Today* **2019**, *336*, 45−49.
(44) Vittenet, J.; Aboussaoud, W.; Mendret, J.; Pic, J.-S.; Debellefontaine, H.; Lesage, N.; Faucher, K.; Manero, M.-H.; Thibault-Starzyk, F.; Leclerc, H.; Galarneau, A.; Brosillon, S. Catalytic ozonation with γ-Al_2O_3 to enhance the degradation of refractory organics in water. *Appl. Catal., A* **2015**, *504*, 519−532.
(45) Jiang, W.; Yu, Y.; Bi, F.; Sun, P.; Weng, X.; Wu, Z. Synergistic elimination of NO_x and chloroaromatics on a commercial V_2O_5-WO_3/TiO_2 catalyst: Byproduct analyses and the SO_2 effect. *Environ. Sci. Technol.* **2019**, *53*, 12657−12667.
(46) Sun, P.; Chen, J.; Zai, S.; Gao, S.; Weng, X.; Wu, Z. Regeneration mechanism of a deactivated zeolite-supported catalyst for the combustion of chlorinated volatile organic compounds. *Catal. Sci. Technol.* **2021**, *11*, 923−933.
(47) Shen, S. C.; Kawi, S. Mechanism of selective catalytic reduction of NO in the presence of excess O_2 over Pt/Si-MCM-41 catalyst. *J. Catal.* **2003**, *213*, 241−250.
(48) Lichtenberger, J.; Amiridis, M. D. Catalytic oxidation of chlorinated benzenes over V_2O_5/TiO_2 catalysts. *J. Catal.* **2004**, *223*, 296−308.
(49) He, F.; Jiao, Y.; Wu, L.; Chen, X.; Liu, S. Enhancement mechanism of Sn on the catalytic performance of Cu/KIT-6 during the catalytic combustion of chlorobenzene. *Catal. Sci. Technol.* **2019**, *9*, 6114−6123.
(50) Huang, H.; Gu, Y.; Zhao, J.; Wang, X. Catalytic combustion of chlorobenzene over VO_x/CeO_2 catalysts. *J. Catal.* **2015**, *326*, 54−68.
(51) Li, N.; Xing, X.; Cheng, J.; Zhang, Z.; Hao, Z. Influence of oxygen and water content on the formation of polychlorinated organic by-products from catalytic degradation of 1,2-dichlorobenzene over a Pd/ZSM-5 catalyst. *J. Hazard. Mater.* **2021**, *403*, No. 123952.
(52) Wang, J.; Wang, X.; Liu, X.; Zhu, T.; Guo, Y.; Qi, H. Catalytic oxidation of chlorinated benzenes over V_2O_5/TiO_2 catalysts: The effects of chlorine substituents. *Catal. Today* **2015**, *241*, 92−99.
(53) de Rivas, B.; López-Fonseca, R.; González-Velasco, J. R.; Gutiérrez-Ortiz, J. I. On the mechanism of the catalytic destruction of 1,2-dichloroethane over Ce/Zr mixed oxide catalysts. *J. Mol. Catal. A: Chem.* **2007**, *278*, 181−188.
(54) Azis, M. M.; Härelind, H.; Creaser, D. On the role of H_2 to modify surface NO_x species over Ag−Al_2O_3 as lean NO_x reduction catalyst: TPD and DRIFTS studies. *Catal. Sci. Technol.* **2015**, *5*, 296−309.
(55) Ma, L.; Cheng, Y.; Cavataio, G.; McCabe, R. W.; Fu, L.; Li, J. In situ DRIFTS and temperature-programmed technology study on NH_3-SCR of NO over Cu-SSZ-13 and Cu-SAPO-34 catalysts. *Appl. Catal., B* **2014**, *156−157*, 428−437.
(56) Zhang, Y.; Yue, X.; Huang, T.; Shen, K.; Lu, B. In situ DRIFTS studies of NH_3-SCR mechanism over V_2O_5-CeO_2/TiO_2-ZrO_2 catalysts for selective catalytic reduction of NO_x. *Materials* **2018**, *11*, No. 1307.

https://doi.org/10.1021/acs.est.1c08009
Environ. Sci. Technol. 2022, 56, 3719−3728